RAA 2021 Vol. **21** No. **1**, 1(14pp) doi: 10.1088/1674-4527/21/1/1

http://www.raa-journal.org *http://iopscience.iop.org/raa*

***R**esearch in*
***A**stronomy and*
***A**strophysics*

Radiative hydrodynamic simulations of the spectral characteristics of solar white-light flares

Yu-Tong Yang[1,2], Jie Hong[3], Ying Li[1,2], Ming-De Ding[3] and Hui Li[1,2]

[1] Key Laboratory of Dark Matter and Space Astronomy, Purple Mountain Observatory, Chinese Academy of Sciences, Nanjing 210033, China; *yingli@pmo.ac.cn*
[2] School of Astronomy and Space Science, University of Science and Technology of China, Hefei 230026, China
[3] School of Astronomy and Space Science, Nanjing University, Nanjing 210023, China; *jiehong@nju.edu.cn*

Received 2020 June 10; accepted 2020 June 26

Abstract As one of the most violent activities in the solar atmosphere, white-light flares (WLFs) are generally known for their enhanced white-light (or continuum) emission, which primarily originates in the solar lower atmosphere. However, we know little about how white-light emission is produced. In this study, we aim to investigate the response of the continua at 3600 Å and 4250 Å and also the Hα and Lyα lines during WLFs modeled using radiative hydrodynamic simulations. We take non-thermal electron beams as the energy source for the WLFs in two different initial atmospheres and vary their parameters. Our results show that the model with non-thermal electron beam heating clearly shows enhancements in the continua at 3600 Å and 4250 Å as well as in the Hα and Lyα lines. A larger electron beam flux, a smaller spectral index, or an initial penumbral atmosphere leads to a stronger emission increase at 3600 Å, 4250 Å and in the Hα line. The Lyα line, however, is more obviously enhanced in a quiet-Sun initial atmosphere with a larger electron beam spectral index. It is also notable that the continua at 3600 Å and 4250 Å and the Hα line exhibit a dimming at the start of heating and reach their peak emissions after the peak time of the heating function, while the Lyα line does not show such behaviors. These results can serve as a reference for the analysis of future WLF observations.

Key words: methods: numerical — radiative transfer — Sun: atmosphere — Sun: flares

1 INTRODUCTION

It is generally acknowledged that solar flares are among solar activities one of the most interesting and intriguing phenomena. Solar white-light flares (WLFs) are a type of solar flares characterized by an enhancement to the optical continuum. They are regarded as the most violent and energetic flare events. However, in general, WLFs are relatively rare since the first report by Carrington (1859), with a very small recorded number compared to the total number of recorded solar flares. The first space observation of WLFs was reported by Hudson et al. (1992) using the Soft X-ray Telescope (Yohkoh/SXT; Tsuneta et al. 1991). WLFs are more prone to arise in the neighborhood of sunspots, which can facilitate the emission enhancement in visible continuum that originates in the solar lower atmosphere (Ding & Fang 1996; Hudson et al. 2006; Jess et al. 2008; Wang 2009). A comprehensive review of the history of WLF research has been presented by Hudson (2016).

With the emergence of more ground-based white-light telescopes and solar satellites which can observe in a wave-band including the optical range, such as Yohkoh/SXT, the Transition Region and Coronal Explorer (TRACE) and the Solar Optical Telescope (Hinode/SOT), more studies have been aimed at the spectral characteristics and possible mechanisms of WLFs. Liu et al. (2001) found that a flare on 2001 March 10 with a continuum enhancement near the Ca II 8542 Å line exhibited a temporal correlation with the peak of the flux at 7.58 GHz. Chen & Ding (2005) showed that the continuum enhancement has a fine co-temporal feature associated with the hard X-ray (HXR) emission produced by bremsstrahlung (Brown 1971) of the non-thermal electrons. Jing et al. (2008) studied a WLF on 2006 December 13 and the results show that the continuum emission enhancements during WLFs are co-spacial to the place where the most energy is deposited from non-thermal electrons which are accelerated by magnetic reconnection (Neidig & Kane 1993; Matthews et al. 2003;

Metcalf et al. 2003; Hudson et al. 2006; Chen & Ding 2006; Fletcher et al. 2007). Moreover, Neidig et al. (1993), Xu et al. (2006) and Isobe et al. (2007) indicate that there is often a core-halo structure of WLF emission, namely a brighter core emission encircled by a fainter and diffused halo. This observational property implies complex components of WLF emission that are related to different heating mechanisms, i.e., direct heating by non-thermal electrons and back-warming. Namekata et al. (2017) studied 50 solar WLFs and examined the correlation between their energies and durations. The result reveals that this relation is similar to that on stellar superflares, in spite of the longer durations but much less energies of solar WLFs than those of stellar superflares. Hao et al. (2017) identified white-light emission in a circular flare and found an impulsive and a gradual white-light kernels (Kane et al. 1985) which might be related to different heating mechanisms. Song et al. (2018) found a standard fan-spine magnetic field configuration (Sun et al. 2013) of a circular-ribbon flare with white-light emission.

The possible radiation mechanisms of white-light continua include recombination radiation (free-bound radiation) of hydrogen atoms in the lower chromosphere and negative hydrogen ion emission in the upper photosphere (Ding et al. 1994). According to the different spectral features in the observational data, there are two types of WLFs which are suspected to have different emission mechanisms (e.g., Machado et al. 1986). Type I WLFs show a Balmer jump, a strong emission of hydrogen lines, and a temporal correlation with HXR emission, while type II WLFs rarely have such features, with the exception that Procházka et al. (2018) stated that type II WLFs can also show a temporal correlation between Balmer emission and HXR emission.

Type I WLFs may be heated by non-thermal electron beams followed by radiative back-warming. Type II WLFs are probably locally heated and can be produced by magnetic reconnection in the lower atmosphere (Machado et al. 1989; Li et al. 1997). Apart from local heating, the possible heating mechanisms for type II WLFs also include bombardment by energetic electron beams with quite a large spectral index and energy transport through Alfvén waves. However, problems such as the energy deposition process in WLFs are not fully solved yet. Until now, many heating mechanisms have been proposed to describe the energy deposition in the temperature minimum region (TMR) and the upper photosphere, which include heating by non-thermal electron beams (Hudson 1972; Aboudarham & Henoux 1986), proton beams (Machado et al. 1978), the dissipation of Alfvén waves (Emslie & Sturrock 1982; Fletcher & Hudson 2008) and chromospheric condensation (Machado et al. 1989; Gan & Mauas 1994). In this paper, we focus on the non-thermal electron beam heating mechanism and use this model to simulate the WLFs. The rationale for this lies in the well correlated continuum enhancements and HXR emission, both spatially and temporally, reported in previous observations of WLFs (Watanabe et al. 2010; Krucker et al. 2015; Kuhar et al. 2016). In fact, the quantitative relationship between non-thermal electrons and white-light emission has been investigated in a number of studies from an observational perspective (Chen & Ding 2005; Fletcher et al. 2007; Kuhar et al. 2016; Watanabe et al. 2017). Recently, Lee et al. (2017) studied an X1.6 flare in AR 12192 on 2014 October 22. They compared the energy flux of non-thermal electrons with the dissipated energy estimated from the Mg II triplet. Their results indicated that the non-thermal electrons can directly produce a continuum enhancement. By studying an X1.8-class flare with strong white-light emission on 2012 October 23, Watanabe & Imada (2020) believed that accelerated electrons could be the source of the white-light emission. These works support the rationale for our simulations.

Since WLFs are believed to originate from a layer deep in the solar atmosphere (e.g., Machado & Rust 1974; Rust & Hegwer 1975), which is characterized by low temperature, high density and partial ionization, obtaining the physical parameters of such a flare atmosphere from the spectral observations is a very complex problem. To uncover the physical mechanisms behind WLFs, we need to resort to sophisticated simulations of the flaring atmosphere by including as many as possible of the key physical processes such as gas dynamics and radiative transfer. With such simulations, we can learn how the continuum emission and the spectral lines, respond to atmospheric heating, in particular by an electron beam, and what spectral characteristics can be used to diagnose the parameters of the electron beam.

In recent years, radiative hydrodynamic simulation has been an important tool to study solar and stellar WLFs. Using RADYN simulations, Allred et al. (2005) reported that the line and continuum emissions can show remarkable increases in the optical and UV bands during both moderate and strong flares. Cheng et al. (2010) used RADYN to successfully reproduce the observational white-light enhancements except for the most energetic WLFs. An M-dwarf WLF was modeled with RADYN by Kowalski et al. (2015), in which excessive optical and near UV continuum emission was produced from a hot and dense chromospheric condensation. They also reproduced self-consistently the observed Balmer jump ratio and color temperature for the first time. However, these results came from electron beams with a very high flux of 10^{13} $\mathrm{erg\,cm^{-2}\,s^{-1}}$ for dMe flares, which is very different from the typical value of 10^{11} $\mathrm{erg\,cm^{-2}\,s^{-1}}$

during solar flares. Quite recently, Procházka et al. (2018, 2019) did some simulations using the RADYN code with the concentration on type II solar WLFs, to reproduce the observed X1.0 solar WLF on 2014 June 11 and study the relationship between hydrogen radiative losses and the low-energy cutoff of the electron beams. The authors pointed out that the absence of significant Lyman excess emission with high low-energy cutoff and low fluxes was a prominent spectral feature for type II WLFs. As for the hydrogen lines, Lyα or Hα, a strong relationship between their emission increase and non-thermal electron beams has been reported by Allred et al. (2005) and Procházka et al. (2019). In addition, Kowalski et al. (2017) has noted the importance of high fluxes of non-thermal electron beam in the broadening of the Balmer lines.

In this paper, we carry out RADYN simulations to study the response of the flaring atmosphere to non-thermal electron beams which has been proved to play an important role in increasing continuum emissions (Allred et al. 2005; Hudson et al. 2006; Jess et al. 2008; Cheng et al. 2010; Procházka et al. 2018). The continua at 3600 Å and 4250 Å, i.e., below and above the Balmer jump at 3646 Å respectively, are calculated here. We also include the Hα and Lyα lines that are formed ranging from the photosphere to the chromosphere and even the transition region (Vernazza et al. 1981) to gain a more comprehensive understanding of the features of the flaring atmosphere. Note that the continua at 3600 Å and 4250 Å are two wavelengths that are used in the Optical and Near-infrared Solar Eruption Tracer (ONSET; Fang et al. 2013) observations. Moreover, the continuum at 3600 Å and the Lyα line are two available observation wavebands for the future LST/ASO-S telescope (Lyman-alpha Solar Telescope/Advanced Space-based Solar Observatory, Li et al. 2019). Therefore, the theoretical calculation can be used as a reference for analyzing future WLF observations.

Here we briefly introduce the numerical method used in our study in Section 2. In Section 3, we present the simulation results of the continua at 3600 Å and 4250 Å, together with the Hα and Lyα lines in response to varying the electron beams. Finally, the discussions and conclusions are given in Section 4.

2 NUMERICAL METHOD

2.1 Flare Simulation

The one-dimensional (1D) non-local thermodynamic equilibrium (non-LTE) radiative hydrodynamics code, RADYN, uses a self-adaptive grid (Dorfi & Drury 1987) to implicitly solve hydrodynamic and radiative transfer equations (Carlsson & Stein 1992, 1995, 1997, 2002). More details about recent implementations can be found in Allred et al. (2015). In this work, we employ this code to calculate the atmospheric response to non-thermal electron beams with different parameters during WLFs, which has been proven practicable and reasonable in the studies mentioned above.

We assume that energy is injected at the top of the flare loop in the form of a non-thermal electron beam and that the loop extends for a length of 10 Mm from the photosphere to the corona with a quarter-circular structure. Electrons then propagate downwards and deposit their energy and momentum in the lower atmosphere to heat and ionize the ambient plasma. The heating rate of the electron beam is quantified by solving the Fokker-Planck equation (McTiernan & Petrosian 1990; Allred et al. 2015). Atoms that show great significance to the chromospheric energy balance are treated in non-LTE. More specifically, hydrogen and Ca II atoms are modeled with six levels including a continuum level, and helium atoms are modeled with nine levels including continuum. All radiative transitions between these levels are calculated in detail and assumed to be under complete frequency redistribution (CRD) to simplify the calculation. Other atoms are treated in LTE and are included in the calculation by means of the Uppsala opacity package (Gustafsson 1973). The return current is not included in the simulations for the following two reasons: (1) the return current only has a large impact on coronal heating (Allred et al. 2015) and does not significantly affect the response of continua or the spectral lines that are formed in the chromosphere or photosphere; (2) non-thermal electron beam heating may considerably outweigh return current heating in the chromosphere. An extra cooling term due to thermal bremsstrahlung and metal collisionally-excited transitions is added into the internal energy conservation equation to include optically thin radiative cooling. This cooling term is obtained from the CHIANTI atomic database (Dere et al. 1997, 2019).

Taking into account the fact that solar WLFs often arise in or near sunspots, we adopt a penumbral atmospheric model for the initial atmosphere (Hong et al. 2018), which is constructed based on the semi-empirical model of Ding & Fang (1989). For comparison, we also employ a quiet-Sun model based on the VAL3C atmosphere (Vernazza et al. 1981) which has been used in some previous works (Hong et al. 2017, 2018, 2019). The main difference between these two model atmospheres is that the penumbral model features a lower temperature in the lower atmosphere, whereas it features a higher temperature in the higher atmosphere, which can be seen in Figure 1.

In our simulations, we assume that the initial atmospheres are heated by electron beams during a flare. The electron beams are assumed to have a power-law distribution with two different spectral indices of

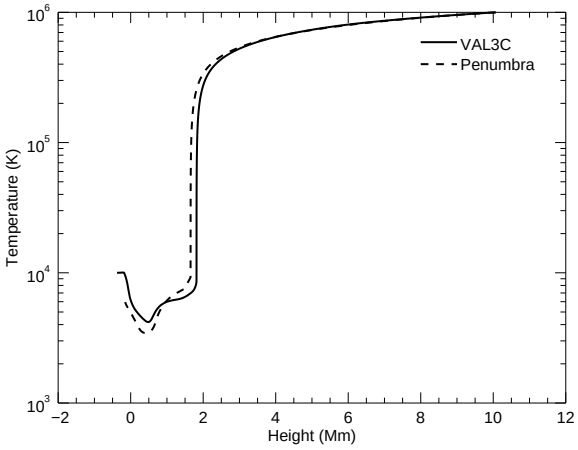

Fig. 1 Temperature distribution of the initial atmosphere after relaxation. The black curve is for the quiet-Sun (VAL3C) and the dashed curve is for the penumbra.

$\delta = 3$ and 5 and a low-energy cutoff of $E_c = 25$ keV. These parameters are selected based on the WLF studies by Kuhar et al. (2016), Fletcher et al. (2007), and Watanabe et al. (2010). The former found that the observed spectral indices of 43 WLFs were mainly between 2.5 and 5.5, and the latter two demonstrated that an electron beam with a low-energy cutoff of around 20–30 keV was sufficient to power the flare WL enhancement. The energy flux of the beam follows a triangular function over time, with a total duration of 20 s. We consider five different average energy fluxes (half of the maxima), $F = 10^9$, 3×10^9, 10^{10}, 3×10^{10}, 5×10^{10} erg cm^{-2} s^{-1}, which are denoted by F9, 3F9, F10, 3F10 and 5F10, respectively. This range of energy fluxes represents variation from a relatively weak flare to a powerful one (Abbett & Hawley 1999). We run all the cases for two different spectral indices, five different energy fluxes, as well as two different initial atmospheres. This means that we have 20 different sets of parameter combinations. Note that here we only consider a disk position of $\mu = 0.953$ (around the disk center). The model parameters of all 20 cases are listed in Table 1. Each case is run for 20 s and the simulation snapshots are saved every 0.1 s. It should be mentioned that performing radiative hydrodynamic simulations of flares even for a 1D model, is computationally challenging and time-consuming, in particular with a higher heating rate and a larger spectral index. Therefore, in our work, we did not finish the computation in some cases, i.e., 3F10d5Q, 5F10d5Q, 3F10d5P, and 5F10d5P, which can be seen in all of the result figures.

Table 1 List of Parameters of Our Simulations

Label	F (erg s^{-1} cm^{-2})	δ	Initial Atmosphere
F9d3Q	10^9	3	Quiet Sun
3F9d3Q	3×10^9	3	Quiet Sun
F10d3Q	10^{10}	3	Quiet Sun
3F10d3Q	3×10^{10}	3	Quiet Sun
5F10d3Q	5×10^{10}	3	Quiet Sun
F9d5Q	10^9	5	Quiet Sun
3F9d5Q	3×10^9	5	Quiet Sun
F10d5Q	10^{10}	5	Quiet Sun
3F10d5Q	3×10^{10}	5	Quiet Sun
5F10d5Q	5×10^{10}	5	Quiet Sun
F9d3P	10^9	3	Penumbra
3F9d3P	3×10^9	3	Penumbra
F10d3P	10^{10}	3	Penumbra
3F10d3P	3×10^{10}	3	Penumbra
5F10d3P	5×10^{10}	3	Penumbra
F9d5P	10^9	5	Penumbra
3F9d5P	3×10^9	5	Penumbra
F10d5P	10^{10}	5	Penumbra
3F10d5P	3×10^{10}	5	Penumbra
5F10d5P	5×10^{10}	5	Penumbra

2.2 Calculation of the Lyα Line

RADYN assumes all transitions in CRD. However, for Lyα line, the partial frequency redistribution (PRD) effects are crucial since the simplified CRD calculation can notably overestimate the radiative losses in strong resonance lines, which causes a false atmospheric temperature structure. Examples can be found in Ulmschneider et al. (1987) and Uitenbroek (2002) for Mg II k or Ca II H & K cases. The effects of PRD on the Lyα line have been shown in Hong et al. (2019) and Kerr et al. (2019a). Motivated by these two studies, we employ the radiative transfer code RH (Uitenbroek 2001; Pereira & Uitenbroek 2015) to calculate the Lyα line profiles. Note that RH assumes the atmosphere to be in statistical equilibrium, which means it does not perfectly satisfy the condition of the highly dynamic impulsive phase in WLFs (Carlsson & Stein 2002). However, the effect of this assumption is not as strong as that of PRD, as discussed by Kerr et al. (2019a,b). Here, for each case, we take snapshots every 0.1 s of the RADYN outputs containing hydrogen level populations and electron density as inputs to the RH code to calculate the Lyα line profiles.

3 SIMULATION RESULTS

3.1 Continuum Contrast

We calculate the continuum contrast for different models, which is defined as $\Delta I/I_0 = (I - I_0)/I_0$ where I and I_0 are the continuum intensities for the flare and pre-flare atmospheres, respectively. Figures 2 and 3 present time evolutions of the continuum contrasts at 3600 Å and 4250 Å with various combinations of initial atmosphere, average energy flux F and spectral index δ. We can see

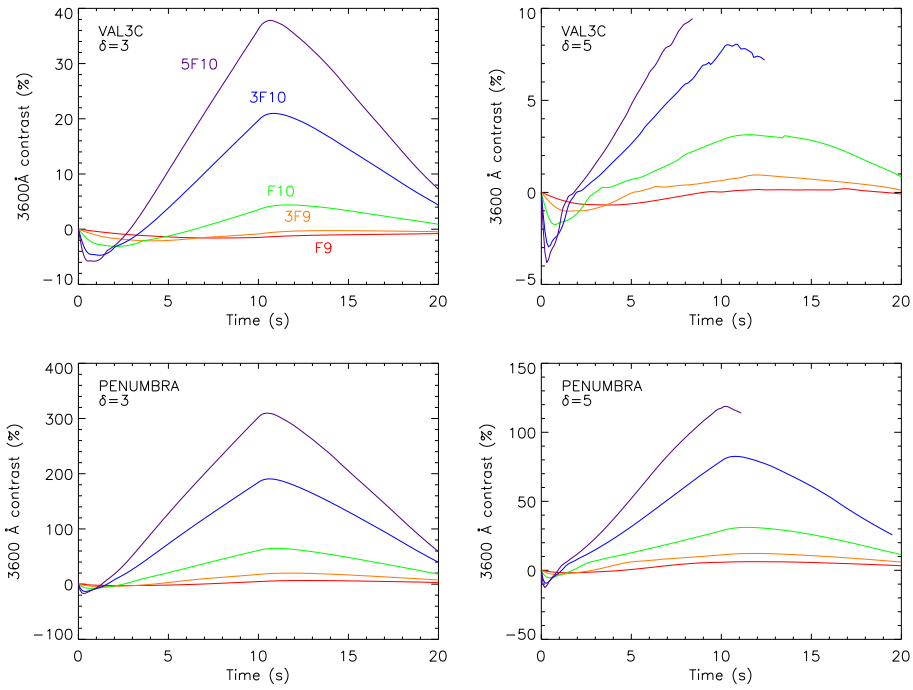

Fig. 2 Time evolution of the continuum contrast at 3600 Å with various combinations of initial atmosphere, average energy flux F and spectral index δ.

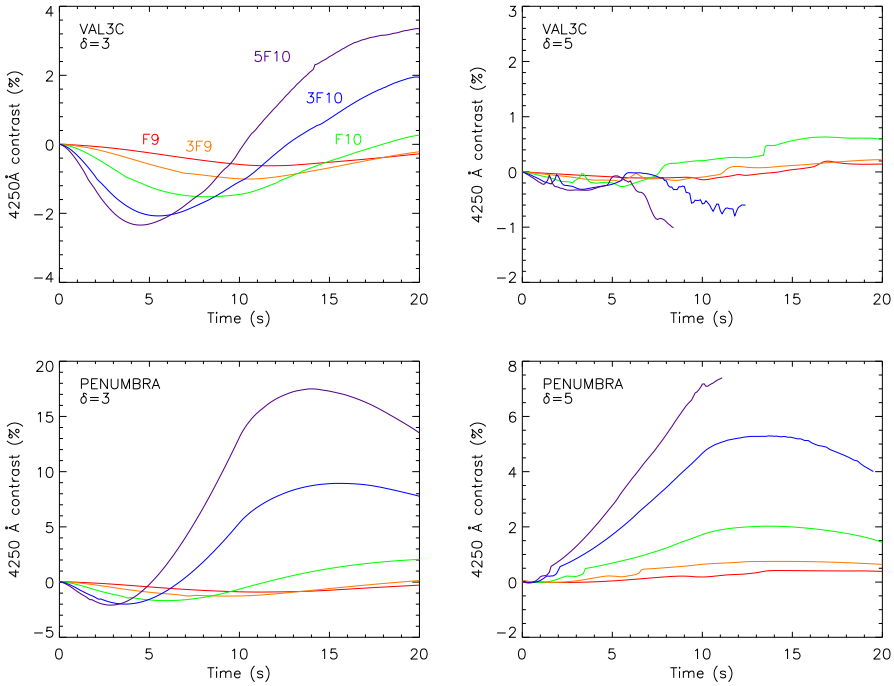

Fig. 3 Same as Fig. 2 but for the continuum contrast at 4250 Å.

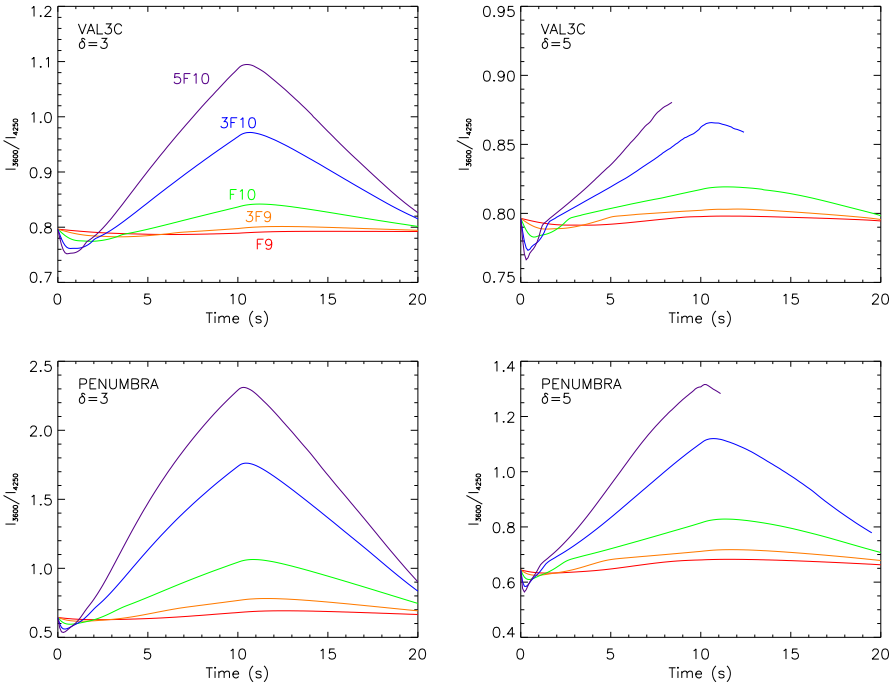

Fig. 4 Time evolution of the ratio of I_{3600}/I_{4250} with various combinations of initial atmosphere, average energy flux F and spectral index δ.

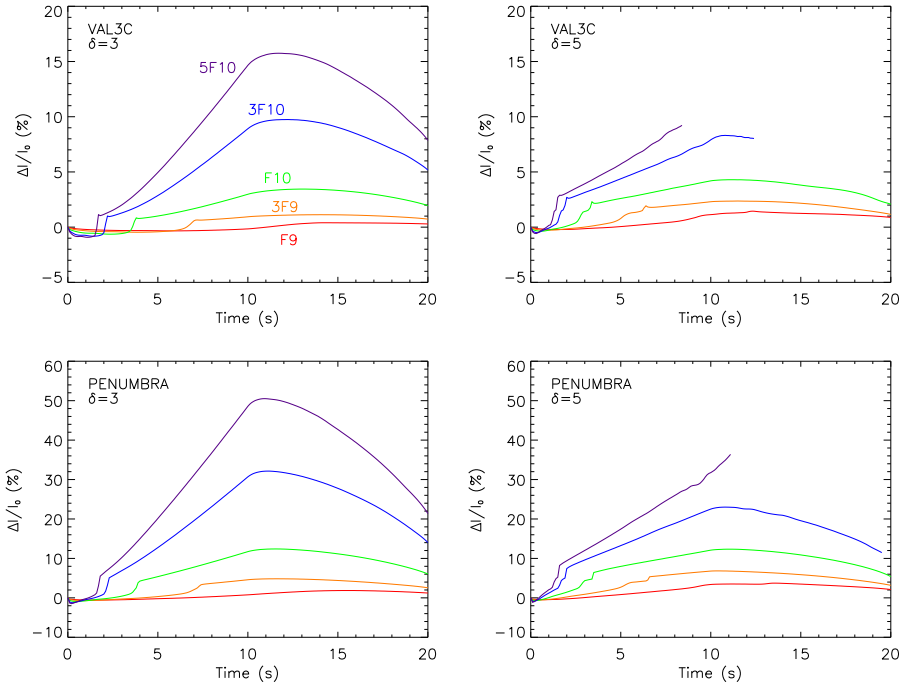

Fig. 5 Time evolution of the integrated intensity contrast of the Hα line with various combinations of initial atmosphere, average energy flux F and spectral index δ. The integration range is from 6520.5 Å to 6609.1 Å.

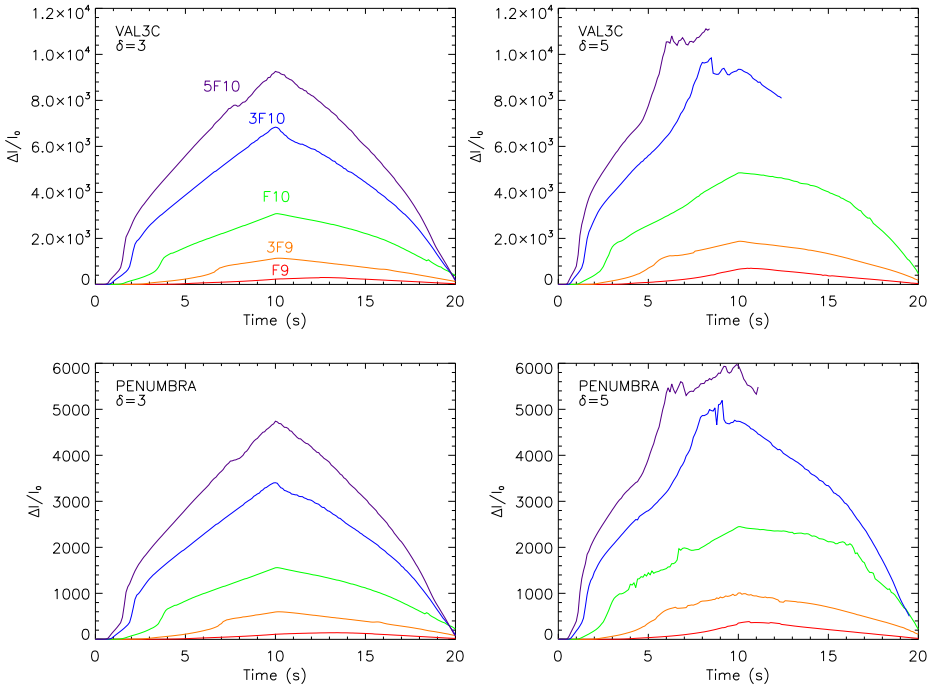

Fig. 6 Same as Fig. 5 but for the Lyα line with an integration range from 1215.0 Å to 1216.5 Å.

that both of the continuum emissions are enhanced as heating takes effect. The enhancement at both wavelengths is greater with a larger flux of the injected electron beam, a smaller spectral index and a penumbral atmosphere. The difference in the enhancement is particularly obvious when the initial atmosphere and electron flux change. For instance, for cases with $\delta = 3$ and quiet-Sun atmosphere, the two highest fluxes result in a continuum contrast at 3600 Å of more than 20%. However, the two lowest fluxes show hardly any enhancement during heating. The effect of initial atmosphere can be seen when cases 3F10d3Q and 3F10d3P are compared. The former exhibits a 3600 Å contrast of slightly more than 20%, while the latter shows a contrast near 200%. We also find that the enhancement of the continuum at 4250 Å is less than that of continuum at 3600 Å. In terms of the percentage of enhancement, the former is one order of magnitude smaller than the latter. For example, in the case of 5F10d3P, the continuum enhancement at 4250 Å is about 17%, while for 3600 Å the value is around 300%.

It can also be seen that at the beginning of the heating, the continua at both 3600 Å and 4250 Å undergo a dimming, with durations and strengths of the dimming varying with the model parameters. The dimming timescale of 4250 Å is longer than that at 3600 Å. This can clearly be seen in the cases with a spectral index of 3 (Figs. 2 and 3). For these cases, the typical duration of dimming at 3600 Å is less than 3 s, while at 4250 Å, almost all the dimming lasts for at least 5 s. Cases with higher electron beam fluxes display shorter dimming periods, and the strength of the dimming shows a negative correlation with its duration. Cases with a quiet-Sun initial atmosphere exhibit a longer duration than those with a penumbral atmosphere. Since the dimming time can be very long in some cases with low energy fluxes (sometimes even more than 10 s, for example, the case F10d3Q), the light curve is still increasing at the end of heating.

In addition, we calculate the ratio of the intensity at 3600 Å to that at 4250 Å (i.e., I_{3600}/I_{4250}, as shown in Fig. 4), which reflects the intensity variation below and above the Balmer jump to some extent. It is seen that this ratio is less than unity before heating. When heating takes place, the enhancement percentage at 3600 Å is one order of magnitude higher than that at 4250 Å, so the curve for this ratio has a shape similar to that for the contrast at 3600 Å, with an initial decrease followed by an increase to a peak value at over 10 s after heating. However, with a penumbral initial atmosphere, a higher energy flux and a smaller spectral index, we can get a larger ratio of I_{3600}/I_{4250}. The maximum ratio found from among all the cases is about 2.3 for the 5F10d3P run. It should be mentioned that the ratio can more easily exceed unity when the penumbral initial atmosphere is applied.

3.2 Hα and Lyα Integrated Intensity

Figures 5 and 6 show the time evolution of the integrated intensity contrasts of the Hα and Lyα lines for different models, which have a similar definition to the continuum contrast. From these two figures, we can find that for quiet-Sun and penumbral initial atmospheres, the integrated intensity contrasts for both Hα and Lyα lines can reflect the effect of electron beam bombardment, since all curves exhibit an increase in the first 10 s. As the electron beam flux increases, the emission of the lines also increases. However, the Hα and Lyα lines do not peak synchronously. For the Hα line, the peak time in all cases is apparently later than 10 s, which is the peak time of the electron energy flux. While for the Lyα line, the intensity peaks at the peak time of the electron energy flux.

The initial atmosphere has also a significant influence on the results. We notice that the enhancement in the Lyα intensity is larger when the quiet-Sun model is used (Fig. 6), whereas for the Hα line the penumbral model displays a stronger enhancement of the line intensity (Fig. 5). The peak values of the contrast for the Hα line in the penumbral atmosphere are basically three times larger than the peak values in the quiet-Sun atmosphere. By contrast, the peak values of the Lyα line in the quiet-Sun atmosphere are roughly twice the peak values in the penumbral atmosphere.

We can also check the effects of the spectral index. By comparing the left and right panels of Figure 6, we can find that the Lyα line shows a greater enhancement when the spectral index is larger, which corresponds to a softer energy spectrum of non-thermal electrons. However, as shown in Figure 5, the Hα line displays a contrary mode: a larger enhancement can be achieved when a harder electron spectrum is applied.

From Figure 5, we can also see that the Hα line exhibits a dimming when the injection of non-thermal electrons begins, which is consistent with the pattern shown in continuum emission. Its dimming timescale is the same as the timescale for the continuum at 3600 Å. When the spectral index gets smaller, the dimming is more significant and lasts longer. A larger electron beam flux is likely to cause a more evident dimming with a shorter duration time. However, looking at Figure 6, no dimming can be found in the Lyα line. This difference is explained in Section 4.

An electron beam with a larger flux should cause an earlier enhancement and a larger peak value. Compared with the Hα line, the enhancement of the Lyα line is more significant. Taking the two cases of 5F10d3Q and 5F10d3P as examples, the contrast can reach 4700 times in the penumbral atmosphere and 9000 times in the quiet-Sun atmosphere for the Lyα line; while for the Hα line, the largest contrast would be about 50%. It is also noteworthy that, when the electron flux is 5F10, there is a small "platform" whose slope becomes smaller or even negative before reaching a peak value (see Fig. 6). This "platform" appears at about 8 s and lasts for less than 1 s when the spectral index is 3. When the spectral index is 5, it appears at about 6 s and lasts for about 2 s. This result is consistent with the intensity dip obtained by Hong et al. (2019), in which the occurrence of the "platform" is supposed to be related to the line asymmetry change.

3.3 The Hα and Lyα Line Profiles

We plot the time evolution of the Hα and Lyα line profiles for the different models in Figures 7–8 and Figures 9–10, respectively. By comparing the profiles of the Hα and Lyα lines in different models, it can be found that the electron beam with different parameters (i.e., the average energy flux and spectral index) plays a more effective role in the enhancement of the lines than the initial atmosphere, which is a little different from the enhancement of the continuum emission described in Section 3.1.

In the overall heating process of the flaring atmosphere, there is always a central reversal in the Lyα line profile. For the case with an average energy flux of F10 or below, as the heating continues, the Lyα line center gradually shifts towards the blue wing, and therefore the spectral line profile presents a red asymmetry. This indicates that the Lyα line center is formed at a height where an upward velocity exists (i.e., a chromospheric evaporation layer; see more details in Hong et al. 2019). For the cases with average energy fluxes of 3F10 and 5F10, the Lyα line center displays a blueshift in the first few seconds of heating, resulting in a red asymmetry. However, when the heating continues to a certain extent, at about 10 s and 8 s for 3F10 and 5F10 cases, respectively, the line center changes from a blueshift to a redshift. At the same time, the line profile changes from a red asymmetry to a blue asymmetry. This implies that at this moment, the Lyα line center is formed in a layer where a downflow exists, i.e., a chromospheric condensation layer. To be more specific, the formation height of the Lyα line center decreases to a region where condensation appears, at least in these two cases (Hong et al. 2019). After the asymmetry change, the Lyα line center gradually moves back to the stationary position.

For the Hα line, before heating, the profile exhibits central absorption. When heating is in progress, an emission appears in the Hα line wing. In the case of intense heating, i.e., an average energy flux of 5F10 and a spectral index of 3, the Hα line profile also shows a change from red asymmetry to blue asymmetry, but such a transition occurs later than the case for Lyα under the same flux of

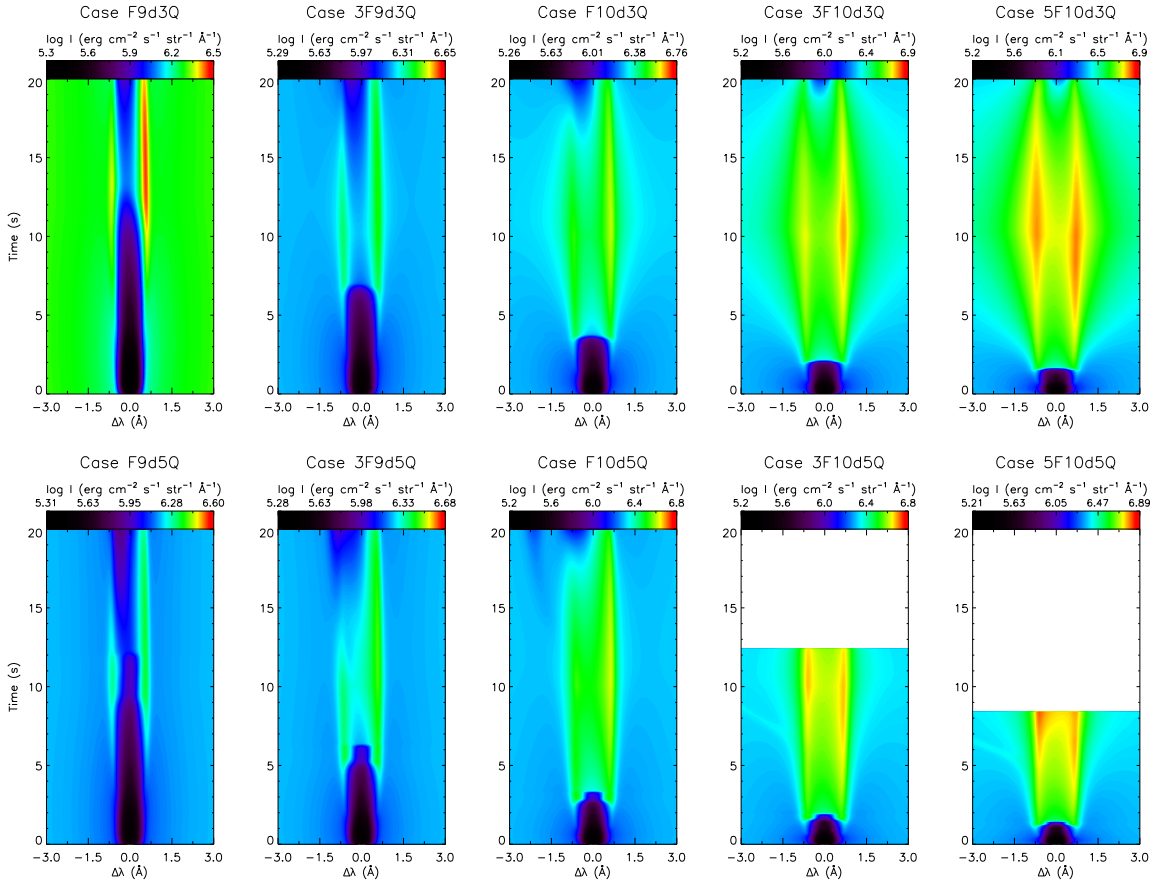

Fig. 7 Time evolution of the Hα line profiles with the quiet-Sun initial atmosphere and spectral index δ = 3 (*top panels*) and 5 (*bottom panels*).

5F10. The former occurs about 10 s after heating starts, in comparison with the latter at about 8 s.

4 DISCUSSIONS AND CONCLUSIONS

In this paper, we carry out radiative hydrodynamic simulations using RADYN to investigate the response of the continua at 3600 Å and 4250 Å together with the Hα and Lyα lines by varying the initial atmospheres and the parameters of the electron beam as the main heating source. We find that the electron beam flux is a very important factor that influences the emission excess of continua and hydrogen lines, especially when it is larger than F10. An important finding is that the electron beam flux is found to influence the enhancement of Hα, Lyα, and continuum in a similar way, whereas the other two factors, the initial atmosphere and the spectral index, show different impacts on the enhancement. For the Hα line as well as the continua at 3600 Å and 4250 Å, an initial penumbral atmosphere and a smaller spectral index can cause a greater emission enhancement, whereas the Lyα line is more favourably enhanced by a quiet-Sun initial atmosphere and a larger spectral index. In addition, it is found that the Lyα line intensity peaks at nearly the same time as the heating function, while the Hα line and the continua at 3600 Å and 4250 Å reach their peak emissions later.

The different responses of the Lyα line with the Hα line as well as the continua at 3600 Å and 4250 Å may be explained by their different formation heights and also the initial atmospheric structure. It is known that the Lyα line is formed from the mid-chromosphere to the low transition region (Vernazza et al. 1981) where the quiet-Sun initial atmosphere has a lower temperature, while the Hα line and the continua at 3600 Å and 4250 Å are formed from the chromosphere to the photosphere (Vernazza et al. 1981) where the initial penumbral atmosphere features a lower temperature in principle. A lower temperature structure should yield a greater emission enhancement. When we consider the effects of the spectral index of the electron beam, these are mainly due to the different depths that electron beams with different spectral indices can penetrate. As reported by Allred et al. (2015), a harder electron beam can deposit its energy into a deeper layer which preferentially enhances spectral lines that form in the lower atmosphere such as Hα, while a softer electron

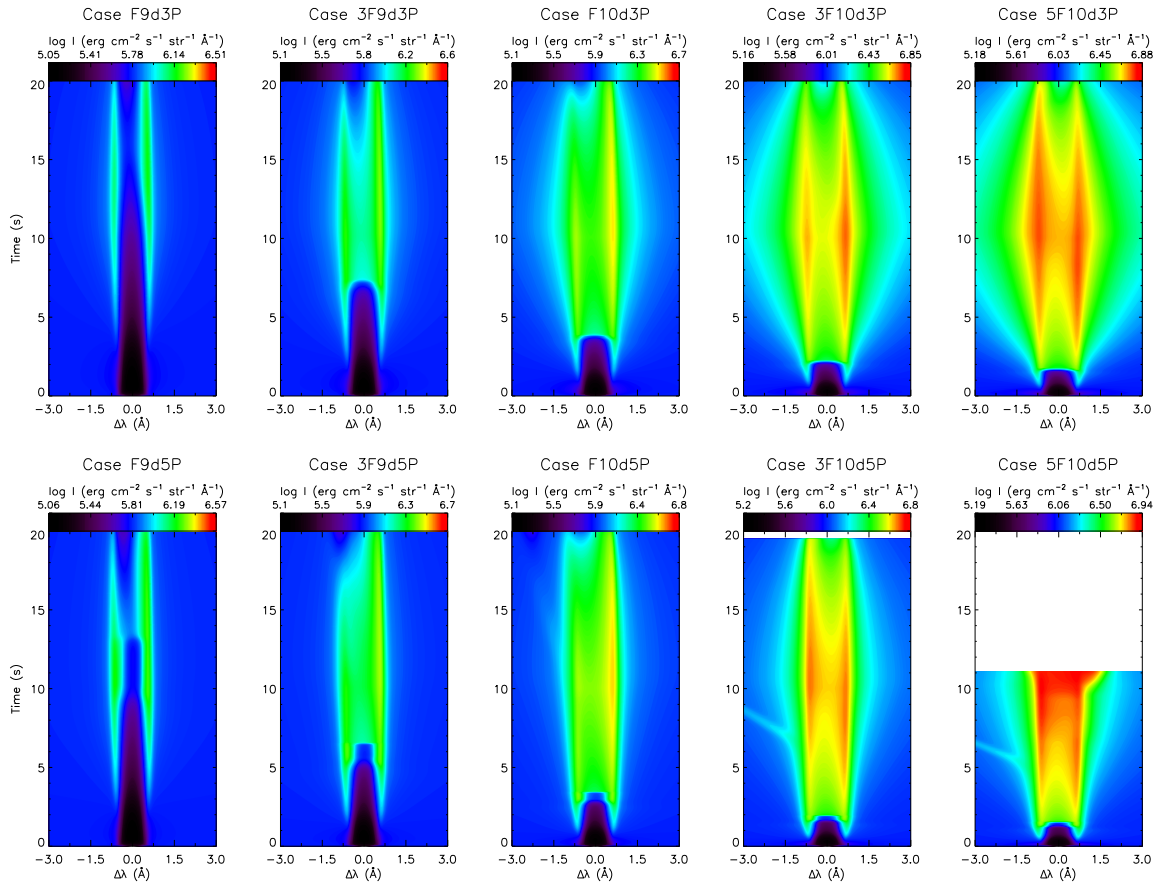

Fig. 8 Same as Fig. 7 but with the initial penumbral atmosphere.

beam deposits its energy into a relatively higher layer that is more favourable for Lyα line emission.

To the best of our knowledge, this is the first time that the response of the continuum at 3600 Å has been calculated, which has already been and will be used in WLF observations. In particular, we calculate the response of the atmosphere through the photosphere to the low transition region for the same electron beam heating regime. The results presented in this work can improve the understanding of the heating mechanisms and energy propagation in WLFs. It is found that the Lyα intensity peaks at nearly the same time as the electron beam heating function in our 20 models. This may suggest that Lyα emission is directly related to non-thermal electron beams. In other words, electron beams mostly deposit their energy in the chromosphere heating the local plasma, and we then see obvious Lyα emission. Subsequently, the continuum at 3600 Å and the Hα line show an emission peak, and finally the continuum at 4250 Å reaches its peak emission. This time sequence may indicate that the deposited energy is transported to the lower atmosphere and successively heats the local plasma. Therefore, we can track the energy propagation from the observed light curves at these wavelengths. It should be noted that cases with a very soft beam or a thermal heating could be different in the processes of energy deposition and propagation (based on a work in preparation).

Furthermore, an initial penumbral atmosphere is employed for the first time to study the response of the continuum emission in the present work, which proves to be more favourable for the enhancement of WL emission compared to the quiet-Sun initial atmosphere. We notice that Cheng et al. (2010) employed a sunspot initial atmosphere in the WLF simulations and these simulations can explain most of the observed WL emissions. The semi-empirical penumbral atmosphere from Ding & Fang (1989) was used to generate the initial atmosphere for the calculations of the Fe I 6173 Å line in a flaring atmosphere by Hong et al. (2018), but it has not been employed for WLF simulations using RADYN code. From our results, it can be found that the initial atmospheres based on different models do cause different simulation outcomes. We find that for both 3600 Å and 4250 Å the enhancement is stronger when the penumbral atmosphere is used. Therefore, we believe that penumbral atmospheric condition, such as a lower temperature at a lower height,

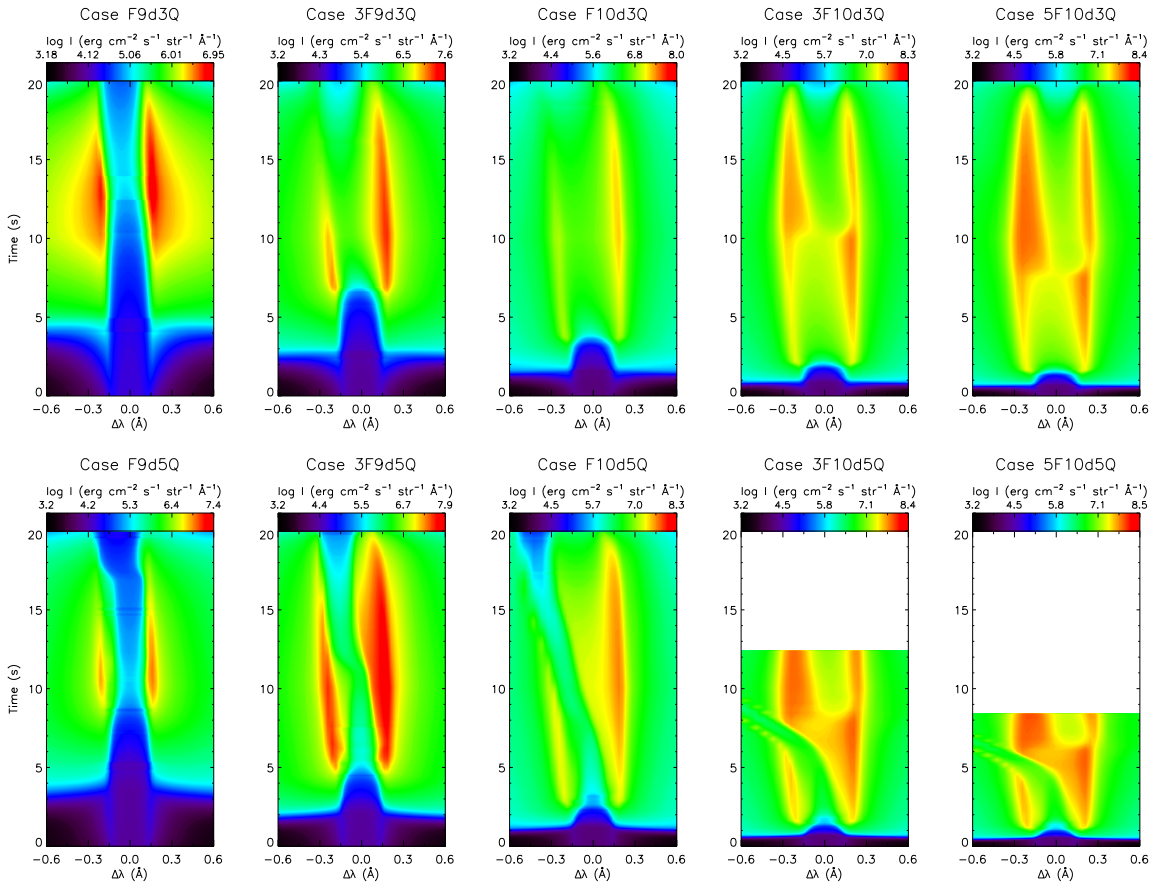

Fig. 9 Same as Fig. 7 but for the Lyα line.

can more easily facilitate WL emission which originates from the lower atmosphere. In fact, this is consistent with the observational fact that solar WLFs usually occur near sunspots or in sunspots.

Our results also imply that a continuum enhancement can be formed in small flares, i.e. with an electron beam flux of strength only F9. Therefore, WLFs can be small flares, which is in agreement with the observational results reported by Hudson et al. (2006). However, a WL emission cannot be produced if the electron beam heating is too short, since there is a dimming of the continuum at the beginning. Note that continuum dimming caused by electron beams has been seen in simulations of solar and stellar flares (Abbett & Hawley 1999; Allred et al. 2006) and also in that of Ellerman bombs (Hong et al. 2017). Such dimming is caused by an over-population of the hydrogen excited levels, and thus an enhanced opacity at the corresponding line and continuum, when atoms are impacted by non-thermal electrons. In particular, the continua at 3600 Å and 4250 Å are mainly contributed by Balmer and Paschen continua, respectively. Therefore, increases in the populations of the first and second excited states of hydrogen cause dimming in the continua at 3600 Å and 4250 Å, respectively.

The duration of the dimming in the continua depends on the trade-off between recombinations and photoionizations (Abbett & Hawley 1999). Over-population of the hydrogen excited levels leads to a higher photoionization rate. However, as flare heating goes on, the electron density in the upper chromosphere is also increased, which raises the recombination rate. Therefore, the over-population of the excited levels is lessened and the continuum begins to brighten. For cases with a stronger electron beam bombardment, the electron density in the heated atmosphere increases more and faster. This leads to an earlier brightening of the continuum, i.e., a shorter dimming. In the meantime, a higher electron beam flux can cause a greater population excess of the hydrogen excited levels, resulting in a stronger dimming. We can see that cases with a quiet-Sun initial atmosphere show a longer dimming than those with a penumbral atmosphere. This is because as the flare evolves, the ratio of recombinations to photoionizations grows more slowly for the quiet-Sun cases, which presents a relatively lower temperature in

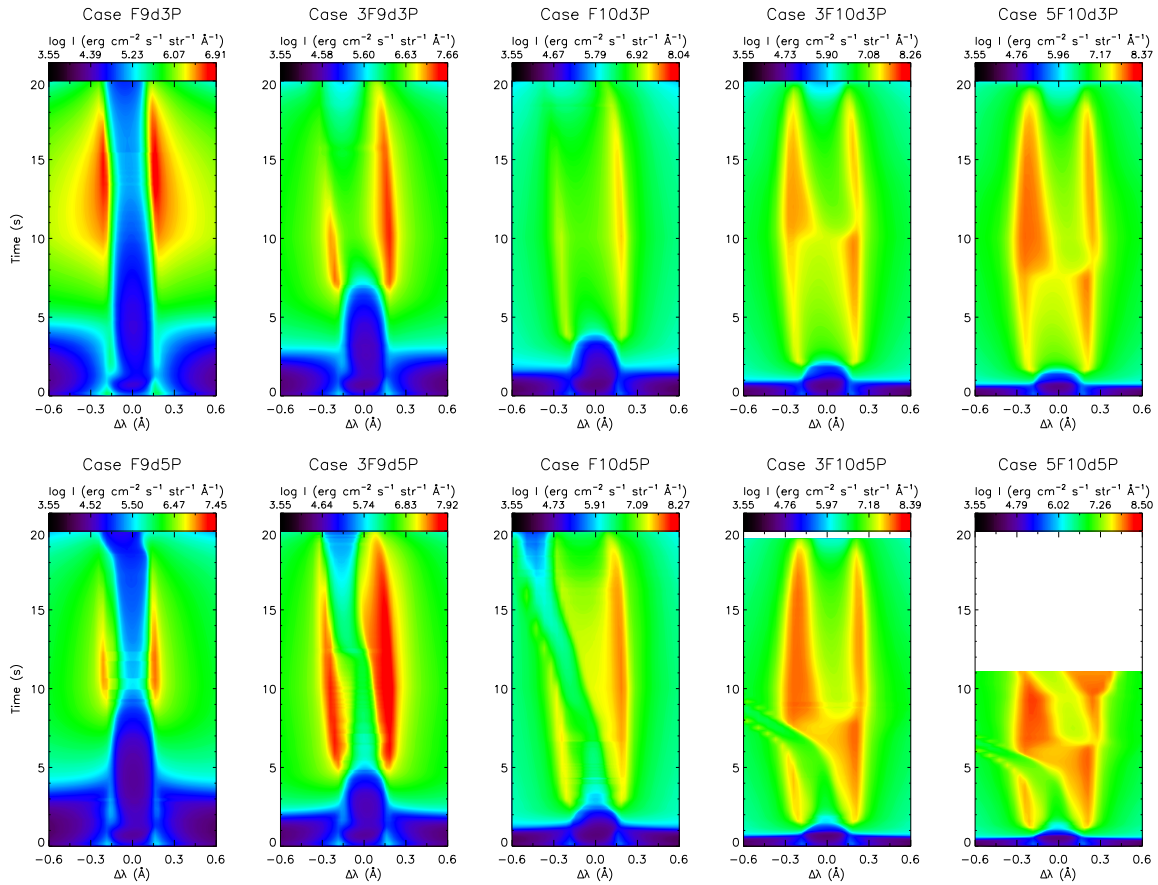

Fig. 10 Same as Fig. 8 but for the Lyα line.

the upper chromosphere and thus a lower ratio of the collisional rate to the photoionization rate.

A threshold of detectable continuum enhancement has been used in the past to identify a WLF, taking into account a practical consideration of instrumental sensitivity in observations. In contrast to the 3% used by Cheng et al. (2010), we assume a threshold of 2%, taking into account the development of detectors in recent years. When the continuum contrast of a flare exceeds this value, this flare is regarded as a WLF. For the continuum at 3600 Å, an F10 electron beam can lead to a detectable enhancement for both spectral indices in the quiet-Sun initial atmosphere. However, for the penumbral atmosphere, the smallest F9 in the flux parameter space is capable of producing a detectable enhancement. As regards the continuum at 4250 Å, when the quiet-Sun initial atmosphere is considered, only a 5F10 electron beam with a spectral index of $\delta = 3$ can reproduce the required enhancement, but for the penumbral atmosphere, a 3F10 electron beam is required for detectable continuum emission for both spectral indices. Note that the required flux is somewhat greater than the value of previously reported by Cheng et al. (2010), which is 3F9 for the continuum at 4300 Å for a disk center event. This discrepancy can be attributed to the difference in the heating function and duration. Here we can see that the flux threshold for continuum at 4250 Å is greater than that at 3600 Å. This is simply because the continuum emission at 4250 Å (the Paschen continuum) originates from a deeper layer than the continuum at 3600 Å (the Balmer continuum) (Kowalski et al. 2015).

As for the Hα and Lyα lines, several previous studies have shown that their excess emission has a strong relationship with non-thermal electron beam bombardment (Allred et al. 2005; Rubio da Costa 2011; Kuridze et al. 2015; Hong et al. 2019; Procházka et al. 2019). Our study broadly supports those studies and provides a theoretical basis from which to interpret future observations. It should be noted that a remarkable difference between the Hα and Lyα lines lies in whether dimming is exhibited by their intensity curves. Hα dimming exists and originates from the increase of the hydrogen population in the first excited state. When electrons penetrate to the lower atmosphere, local hydrogen atoms will be excited to higher energy levels. At the beginning of the heating, the increase of the population of the first excited state typically outweighs

the higher energy states. Therefore, more hydrogen atoms in the first excited state increase the opacity and lead to more absorption at the Hα line, which causes dimming of the line (Abbett & Hawley 1999; Allred et al. 2005). However, for the Lyα line, which is generated by the transition between the first excited state and the ground state of the hydrogen atom, since the ground state is less populated when the atmosphere is bombarded by non-thermal electrons, it does not show any dimming when heating begins.

We have also shown that the Hα and Lyα lines can exhibit an asymmetry and even asymmetry change when the flaring atmosphere is heated by non-thermal beam electrons. In particular, the Lyα line asymmetry changes in coincidence with the light curve "platform". This intensity "platform" has also been shown in previous simulations and called a "dip" (Hong et al. 2019), which is believed to be a mark of non-thermal electron beam heating. For the Hα line, an asymmetry change can also be seen, say, in the model 5F10d3Q at about 10 s. Note that the "platform" in the Hα light curves is generally inconspicuous, which may be due to the fact that the asymmetry change happens near the peak time of electron flux, which also flattens the Hα light curve to some extent. These characteristics visible in the line profiles and also the light curves may serve as a reference for future high-resolution observations.

Considering that the observational wavebands of the future LST/ASO-S telescope include the Lyα line and 3600 Å, our simulations can serve as guidance about how observations should be performed. The high-cadence of LST is expected to observe dimming or black-light flares at a time resolution of 4 s (for 3600 Å, the time resolution can be as short as 1 s), which have rarely been observed before. Moreover, if our simulations can be combined with observations made by the future LST/ASO-S and also the ONSET telescope, which include comprehensive observations in the Lyα, 3600 Å and 4250 Å wavebands, we can expect a diagnosis of the heating mechanism and energy transportation in solar WLFs.

It should be also mentioned that in this work, we only focus on beam heating in a single loop. However, real flares are actually composed of many small-scale threads. Therefore, to facilitate comparison between observations and numerical simulation, multithreaded simulations are required. A multithreaded hydrodynamic model has been employed by Reep et al. (2019) to describe the heating in flares, and some observed spectral properties can be explained by such a model. By considering a series of successively heated loops in the model, Reep et al. (2020) reproduced the observed light curves, quasi-periodic pulsations, and soft X-ray spectra. We expect that some effects may be enhanced and others might be reduced by the use of a multithreaded model. It would be worth trying that kind of model in the future to study solar WLFs.

Finally, our main conclusions can be outlined as follows:

1. The non-thermal electron beam heating model clearly shows enhancements to the continua at 3600 Å and 4250 Å and in the Hα and Lyα lines.
2. A larger electron beam flux, a smaller spectral index or an initial penumbral atmosphere leads to a stronger emission increase at 3600 Å, 4250 Å and in the Hα line, whereas for the Lyα line, a larger spectral index and a quiet-Sun initial atmosphere are preferable conditions for a line-intensity increase.
3. It is also notable that the continua at 3600 Å and 4250 Å and the Hα line exhibit a dimming at the beginning of the heating and reach their peak emissions later than the peak time of the heating function. However, the Lyα line does not show a dimming and reaches its peak emission at nearly the same time as the heating function.
4. Both the Hα and Lyα lines show a change from red asymmetry to blue asymmetry when intense heating exists. Such a change occurs later for Hα compared with Lyα, and the asymmetry change in the Hα line profiles is not as significant as that in Lyα line profiles.

Acknowledgements This work was supported by the National Natural Science Foundation of China (Grant Nos. 11873095, 11903020, 11733003 and U1731241), and by the CAS Strategic Pioneer Program on Space Science (XDA15052200, XDA15320103 and XDA15320301). Y.L. is also supported by the CAS Pioneer Talents Program for Young Scientists.

References

Abbett, W. P., & Hawley, S. L. 1999, ApJ, 521, 906
Aboudarham, J., & Henoux, J. C. 1986, A&A, 156, 73
Allred, J. C., Hawley, S. L., Abbett, W. P., & Carlsson, M. 2005, ApJ, 630, 573
Allred, J. C., Hawley, S. L., Abbett, W. P., & Carlsson, M. 2006, ApJ, 644, 484
Allred, J. C., Kowalski, A. F., & Carlsson, M. 2015, ApJ, 809, 104
Brown, J. C. 1971, Sol. Phys., 18, 489
Carlsson, M., & Stein, R. F. 1992, ApJL, 397, L59
Carlsson, M., & Stein, R. F. 1995, ApJL, 440, L29
Carlsson, M., & Stein, R. F. 1997, ApJ, 481, 500
Carlsson, M., & Stein, R. F. 2002, ApJ, 572, 626
Carrington, R. C. 1859, MNRAS, 20, 13
Chen, Q. R., & Ding, M. D. 2005, ApJ, 618, 537
Chen, Q. R., & Ding, M. D. 2006, ApJ, 641, 1217
Cheng, J. X., Ding, M. D., & Carlsson, M. 2010, ApJ, 711, 185

Dere, K. P., Del Zanna, G., Young, P. R., et al. 2019, ApJS, 241, 22
Dere, K. P., Landi, E., Mason, H. E., et al. 1997, A&AS, 125, 149
Ding, M. D., & Fang, C. 1989, A&A, 225, 204
Ding, M. D., & Fang, C. 1996, Sol. Phys., 166, 437
Ding, M. D., Fang, C., Gan, W. Q., & Okamoto, T. 1994, ApJ, 429, 890
Dorfi, E. A., & Drury, L. O. 1987, Journal of Computational Physics, 69, 175
Emslie, A. G., & Sturrock, P. A. 1982, Sol. Phys., 80, 99
Fang, C., Chen, P.-F., Li, Z., et al. 2013, RAA (Research in Astronomy and Astrophysics), 13, 1509
Fletcher, L., Hannah, I. G., Hudson, H. S., & Metcalf, T. R. 2007, ApJ, 656, 1187
Fletcher, L., & Hudson, H. S. 2008, ApJ, 675, 1645
Gan, W. Q., & Mauas, P. J. D. 1994, ApJ, 430, 891
Gustafsson, B. 1973, Uppsala Astron. Obs. Ann., 5, 1
Hao, Q., Yang, K., Cheng, X., et al. 2017, Nature Communications, 8, 2202
Hong, J., Carlsson, M., & Ding, M. D. 2017, ApJ, 845, 144
Hong, J., Ding, M. D., Li, Y., & Carlsson, M. 2018, ApJL, 857, L2
Hong, J., Li, Y., Ding, M. D., & Carlsson, M. 2019, ApJ, 879, 128
Hudson, H. S. 1972, Sol. Phys., 24, 414
Hudson, H. S. 2016, Sol. Phys., 291, 1273
Hudson, H. S., Acton, L. W., Hirayama, T., & Uchida, Y. 1992, PASJ, 44, L77
Hudson, H. S., Wolfson, C. J., & Metcalf, T. R. 2006, Sol. Phys., 234, 79
Isobe, H., Kubo, M., Minoshima, T., et al. 2007, PASJ, 59, S807
Jess, D. B., Mathioudakis, M., Crockett, P. J., & Keenan, F. P. 2008, ApJL, 688, L119
Jing, J., Chae, J., & Wang, H. 2008, ApJL, 672, L73
Kane, S. R., Love, J. J., Neidig, D. F., & Cliver, E. W. 1985, ApJL, 290, L45
Kerr, G. S., Allred, J. C., & Carlsson, M. 2019a, ApJ, 883, 57
Kerr, G. S., Carlsson, M., & Allred, J. C. 2019b, ApJ, 885, 119
Kowalski, A. F., Hawley, S. L., Carlsson, M., et al. 2015, Sol. Phys., 290, 3487
Kowalski, A. F., Allred, J. C., Uitenbroek, H., et al. 2017, ApJ, 837, 125
Krucker, S., Saint-Hilaire, P., Hudson, H. S., et al. 2015, ApJ, 802, 19
Kuhar, M., Krucker, S., Martínez Oliveros, J. C., et al. 2016, ApJ, 816, 6
Kuridze, D., Mathioudakis, M., Simões, P. J. A., et al. 2015, ApJ, 813, 125
Lee, K.-S., Imada, S., Watanabe, K., Bamba, Y., & Brooks, D. H. 2017, ApJ, 836, 150
Li, H., Chen, B., Feng, L., et al. 2019, RAA(Research in Astronomy and Astrophysics), 19, 158
Li, X. Q., Song, M. T., Hu, F. M., & Fang, C. 1997, A&A, 320, 300
Liu, Y., Ding, M. D., & Fang, C. 2001, ApJL, 563, L169
Machado, M. E., & Rust, D. M. 1974, Sol. Phys., 38, 499
Machado, M. E., Emslie, A. G., & Brown, J. C. 1978, Sol. Phys., 58, 363
Machado, M. E., Emslie, A. G., & Mauas, P. J. 1986, A&A, 159, 33
Machado, M. E., Emslie, A. G., & Avrett, E. H. 1989, Sol. Phys., 124, 303
Matthews, S. A., van Driel-Gesztelyi, L., Hudson, H. S., & Nitta, N. V. 2003, A&A, 409, 1107
McTiernan, J. M., & Petrosian, V. 1990, ApJ, 359, 524
Metcalf, T. R., Alexander, D., Hudson, H. S., & Longcope, D. W. 2003, ApJ, 595, 483
Namekata, K., Sakaue, T., Watanabe, K., et al. 2017, ApJ, 851, 91
Neidig, D. F., & Kane, S. R. 1993, Sol. Phys., 143, 201
Neidig, D. F., Kiplinger, A. L., Cohl, H. S., & Wiborg, P. H. 1993, ApJ, 406, 306
Pereira, T. M. D., & Uitenbroek, H. 2015, A&A, 574, A3
Procházka, O., Reid, A., Milligan, R. O., et al. 2018, ApJ, 862, 76
Procházka, O., Reid, A., & Mathioudakis, M. 2019, ApJ, 882, 97
Reep, J. W., Bradshaw, S. J., Crump, N. A., & Warren, H. P. 2019, ApJ, 871, 18
Reep, J. W., Warren, H. P., Moore, C. S., et al. 2020, ApJ, 895, 30
Rubio da Costa, F. 2011, Solar Chromospheric Flares: Observations in Ly-lpha and Hlpha and Radiative Hydrodynamic Simulations, PhD Thesis, Max-Planck-Institute for Solar System Research, Max-Planck-Strasse 2, 37191 Katlenburg-Lindau, Germany
Rust, D. M., & Hegwer, F. 1975, Sol. Phys., 40, 141
Song, Y. L., Guo, Y., Tian, H., et al. 2018, ApJ, 854, 64
Sun, X., Hoeksema, J. T., Liu, Y., et al. 2013, ApJ, 778, 139
Tsuneta, S., Acton, L., Bruner, M., et al. 1991, Sol. Phys., 136, 37
Uitenbroek, H. 2001, ApJ, 557, 389
Uitenbroek, H. 2002, ApJ, 565, 1312
Ulmschneider, P., Muchmore, D., & Kalkofen, W. 1987, A&A, 177, 292
Vernazza, J. E., Avrett, E. H., & Loeser, R. 1981, ApJS, 45, 635
Wang, H.-M. 2009, RAA (Research in Astronomy and Astrophysics), 9, 127
Watanabe, K., Krucker, S., Hudson, H., et al. 2010, ApJ, 715, 651
Watanabe, K., Kitagawa, J., & Masuda, S. 2017, ApJ, 850, 204
Watanabe, K., & Imada, S. 2020, ApJ, 891, 88
Xu, Y., Cao, W., Liu, C., et al. 2006, ApJ, 641, 1210